International Journal of Heat and Mass Transfer 103 (2016) 1155–1165

Contents lists available at ScienceDirect

International Journal of Heat and Mass Transfer

journal homepage: www.elsevier.com/locate/ijhmt

Experimental and numerical investigation of constructal vascular channels for self-cooling: Parallel channels, tree-shaped and hybrid designs

O. Yenigun, E. Cetkin *

Izmir Institute of Technology, Department of Mechanical Engineering, Urla, Izmir 35430, Turkey

ARTICLE INFO

Article history:
Received 13 June 2016
Received in revised form 10 August 2016
Accepted 21 August 2016
Available online 28 August 2016

Keywords:
Constructal
Self-cooling
Vascular
Parallel channels
Tree-shaped
Hybrid

ABSTRACT

In this paper, we show experimentally and numerically how a plate which is subjected to a constant heat load can be kept under an allowable temperature limit. Vascular channels in which coolant fluid flows have been embedded in the plate. Three types of vascular channel designs were compared: parallel channels, tree-shaped and their hybrid. The effects of channel design on the thermal performance for different volume fractions (the fluid volume over the solid volume) are documented. In addition, the effects of the number of channels on cooling performance have been documented. Changing the design from parallel channels to tree-shaped designs decreases the order of pressure drop. Hence increase in the order of the convective heat transfer coefficient is achieved. However, tree-shaped designs do not bathe the entire domain, which increases the conductive resistances. Therefore, additional channels were inserted at the uncooled regions in the tree-shaped design (hybrid design). The best features of both parallel channels and tree-shaped designs are combined in the hybrid of them: the flow resistances to the fluid and heat flow become almost as low as the tree-shaped and parallel channels designs, respectively. The effect of design on the maximum temperature shows that there should be an optimum design for a distinct set of boundary conditions, and this design should be varied as the boundary conditions change. This result is in accord with the constructal law, i.e. the shape should be varied in order to minimize resistances to the flows.

1. Introduction

Advanced technologies require great volumetric cooling capabilities especially in miniature designs [1,2]. Heat transfer surface area is limited in miniature designs, therefore, they cannot be cooled down with natural or forced convection when working fluid is air. Therefore, the current literature focuses on heat transfer enhancement with phase changing materials or forced convection with water, oil or nano-fluids working fluids [3–14]. These methods are essential in order to increase the rate of heat transfer. However, heat load can be of two kinds: deterministic and random [15]. In deterministic heating loads, the heating rate and the surface on which the heat flux is applied is known such as electronic circuits. In random type loads, neither heating rate nor on which surface it is applied are known such as thermal runaway phenomenon in accumulators. Advanced technologies require miniature structures with the capability of cooling itself under deterministic and random heating loads. This requirement can be satisfied with self-cooling structures, which can be obtained by embedding vascular channels inside the body [15–19].

Materials with smart features first suggested by White et al. [20] in 2001. They mimicked the self-healing mechanism of animals, i.e. clot occurrence at the wound in order to seal it. In their autonomic healing concept, healing agents were placed in spheres which can be used once. Later, Bejan et al. [21] discussed that circulating healing agents in embedded vascular channel network enables structure to heal itself countless time.

Kim et al. [16] showed that vascularized structures can also be used to cool a domain on which heat load is applied. Literature also documents how the pressure drop can be minimized with altering design in parallel channel and tree-shaped designs [16–18]. Because the tree-shaped designs promise lower pressure drop values than parallel channels and radial designs, their cooling performance was surveyed in the literature [22–26]. In our previous study, we also numerically investigated the cooling performance of some parallel channels and tree-shaped configurations [27]. Cho et al. [28] numerically investigated the hydrodynamic and

* Corresponding author.
E-mail address: erdalcetkin@gmail.com (E. Cetkin).

http://dx.doi.org/10.1016/j.ijheatmasstransfer.2016.08.074
0017-9310/

Nomenclature

c_p	specific heat at constant pressure [J kg^{-1} K^{-1}]
d	vascular channel diameter [m]
∇	del operator
$\mathbf{I}$	unit matrix
k_f	thermal conductivity of the coolant fluid [W m^{-1} K^{-1}]
k_s	thermal conductivity of the solid [W m^{-1} K^{-1}]
L	plate width [m]
L_{channel}	distributing/collecting channel length [m]
$\dot{m}$	mass flow rate [kg s^{-1}]
n	vector normal to the fluid–solid interface
P	pressure [Pa]
q''	heat flux [W/m^2]
T	temperature [K]
$\mathbf{u}$	velocity vector

Greek symbols

ΔP	pressure drop [Pa]
φ	volume fraction
μ	dynamic viscosity [kg m^{-1} s^{-1}]
ρ	density [kg m^{-3}]

Subscripts

0,1,2,3	index of tree branches
i	index
max	maximum
min	minimum
peak	peak

Superscripts

n	index of mesh independency test
T	transpose of matrix

thermal performance of vascular designs with embedded parallel channels. They have documented the hydrodynamic and thermal characteristics of three different constructs where the complexity of the parallel channel network was altered. Later, Cho et al. [29] documented the performance of the three parallel channel vascular channel network mentioned in Cho et al. [28] numerically and experimentally. Cho et al. [29] documents the hydrodynamic characteristics of vascular channels in details. They have measured the surface temperature of the vascular plate from several locations via thermocouples, and these locations were chosen in the cooled region (active area). These locations do not correspond to the peak temperature values for each design.

Wang et al. [30] uncovered how the mechanical strength of a solid structure can be increased with embedding vascular channels and how it varies with changing the channel design and volume fraction. Later, Cetkin et al. [31] showed how the mechanical strength and cooling performance is affected by the volume fraction and by the shape of the channel configurations. Cetkin et al. [15] uncovered that vascularization provides required cooling for both deterministic and random heat loads. The current literature also shows how vascularization can increase the mechanical strength of a heated domain, and when the effect of thermal stresses can be neglected [31–33]. In addition to vascular channels on self-cooling structures, Cetkin [34] also documents how high-conductivity inserts on vascular channels effects cooling performance.

Here we show experimentally and numerically how a novel hybrid design gains self-cooling capability to a solid structure with minimum energy consumption, i.e. minimum pumping power requirement. The literature lacks of experimental studies on vascularized structures. This study documents both experimental results and their comparison with numerical study results. In addition, a hybrid of parallel channels and tree-shaped configurations is discussed in order to decrease fluid flow and heat flow resistances by following the principles of Constructal Theory, which is a physical phenomenon that states a flow system should evolve freely in order to adapt to the changing conditions [35–37]. Note that, vascularized structures are proposed as adjunct to the phase changing materials and nano-fluidic cooling methods, not to replace them.

2. Model & numerical method

Consider a plate with embedded vascular cooling channels which is subjected to a constant heat flux from one of its surfaces, as shown in Fig. 1. Coolant fluid flows along the embedded cooling channels. The fluid flow is driven by the pressure difference between the inlet and outlet ports of the vascular network. The volume of the vascular channels and the volume of the solid material are fixed. The outer surfaces of the plate are symmetry boundaries ($\partial T/\partial n = 0$) with only exception of the surface on which heat flux is applied, Fig. 1. The symmetry condition is selected because the plate is an elemental domain of a system which consists a number of identical elements. The coolant fluid is water and its thermo-physical properties as a function of temperature are given in Table 1. In addition, the fluid flow is steady and single phase. With these are in mind, the conservation of mass, momentum and energy equations can be written as

$$\rho\nabla\cdot(\mathbf{u}) = 0 \tag{1}$$

$$\rho(\mathbf{u}\cdot\nabla)\mathbf{u} = \nabla\cdot[-P\mathbf{I} + \mu((\nabla\mathbf{u})^T + \nabla\mathbf{u})] \tag{2}$$

$$\rho c_p\mathbf{u}\nabla T = \nabla\cdot(k_f\nabla T) \tag{3}$$

$$\nabla\cdot(k_s\nabla T) = 0 \tag{4}$$

where ρ, u, μ and P are the fluid density, the velocity vector in the fluid domain, the dynamic viscosity and the pressure, respectively. In addition, ∇ and $\mathbf{I}$ represents del operator and unit matrix. Here T, k and c_p are the temperature, the thermal conductivity and the specific heat at constant pressure. In addition, s and f indices denote solid and fluid. The conservation of the energy at the interfaces require

$$k_f\frac{\partial T}{\partial n}\bigg|_f = k_s\frac{\partial T}{\partial n}\bigg|_s \tag{5}$$

where n is the vector normal to the fluid–solid interface.

Conservation of mass, momentum and energy equations were solved by using a finite element software [38]. First, the plate with parallel cooling channels (semi-circular) was simulated, which is the case discussed in Cho et al. [29], detailed information about the design is given in Table 2. Mesh elements are non-uniform with boundary layer meshes in order to uncover the effect of sudden changes of the gradients near the boundaries. The mesh size was decreased until the criteria of $|(T^n_{\text{peak}} - T^{n+1}_{\text{peak}})/T^n_{\text{peak}}| < 5\times10^{-3}$ and $|(\dot{m}^n_{\text{inlet}} - \dot{m}^{n+1}_{\text{inlet}})/\dot{m}^n_{\text{inlet}}| < 5\times10^{-3}$ are both satisfied. Relative errors corresponding to the mesh size can be seen in Table 3. The residual was imposed as 10^{-6} in the numerical procedure. Table 3 shows

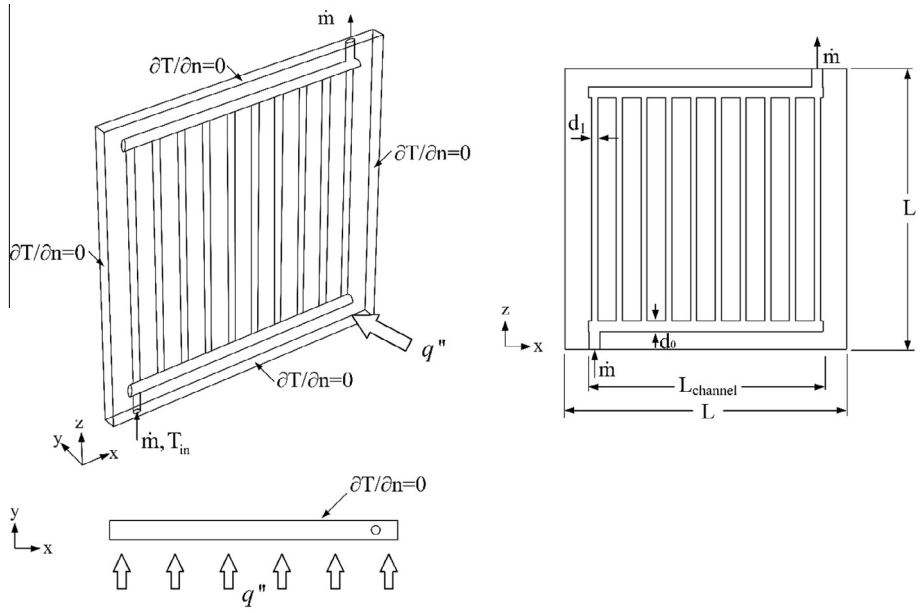

Fig. 1. Geometry and boundary conditions of the vascularized plate with parallel cooling channels.

Table 1
Thermo-physical properties of DI water, AISI 304 and Al5083 at atmospheric pressure [29,38].

	DI Water [29]	AISI 304 [29]	Al 5083 [38]
ρ	998.2	8030.0	2699.5
k	$-0.829 + 0.0079T - 1.04 \times 10^{-5}T^2$	$11.702649 + 0.012955T$	$30.01698 + 0.4662148T - 6.570887 \times 10^{-4}T^2 + 3.182847 \times 10^{-7}T^3$
c_p	$5348 - 7.42T + 1.17 \times 10^{-2}T^2$	$114.227517 + 1.877902T - 0.003234T^2$ $+3.0 \times 10^{-6}T^3 - 8 \times 10^{-10}T^4$	$-263.528 + 9.293216T - 0.01210442T^2$ $-6.74101 \times 10^{-5}T^3 + 1.654763 \times 10^{-7}T^4$
μ	$0.0194 - 1.065 \times 10^{-4}T + 1.489 \times 10^{-7}T^2$	–	–

Table 2
Dimensions of the competitive designs.

	Designs	d_0 [m]	d_1 [m]	d_2 [m]	d_3 [m]
$\varphi = 0.065$	Parallel	0.003338	0.001849	–	–
$L = 0.12$ m	Tree-shaped	0.003338	0.002623	0.002082	0.001653
$L_{ch} = 0.1$ m	Hybrid	0.003338	0.002218	0.001761	0.001397
$\varphi = 0.05$	Parallel	0.004	0.003	–	–
$L = 0.17$ m	Tree-shaped	0.004	0.003	0.0025	0.002
$L_{ch} = 0.15$ m	Hybrid	0.004	0.003	0.0025	0.002

Table 3
Relative errors corresponding to the number of mesh elements.

Number of mesh elements	T_{peak} [K]	$\lvert(T^n_{peak} - T^{n+1}_{peak})/T^n_{peak}\rvert$	$\dot{m}_{inlet}$ [kg/s]	$\lvert(\dot{m}^n_{inlet} - \dot{m}^{n+1}_{inlet})/\dot{m}^n_{inlet}\rvert$
126385	318.13	–	7.28×10^{-4}	–
187142	317.83	9.43×10^{-4}	7.64×10^{-4}	4.97×10^{-2}
261248	317.59	7.55×10^{-4}	7.67×10^{-4}	3.93×10^{-3}

that the solution becomes mesh independent with 261248 mesh elements.

First, the simulation results were validated by using the numerical and experimental data of Cho et al. [29]. Fig. 2 shows that the current study agrees well with the results of Cho et al. [29]. The change in the mass flow rate is maximum 6.60% and 2.95% for numerical and experimental studies in comparison to Cho et al. [29], respectively. In addition, the change in the peak temperatures are 2.14% and 1.23% for pressure drops of 94.8 Pa and 277.9 Pa for numerical studies documented in the study of Cho et al. [29]. Therefore, it is concluded that the simulation results are mesh independent and accurate in comparison with the current literature.

3. Experimental procedure

Next, the performance of the vascularized plates was surveyed experimentally. Fig. 3 shows the schematic of the experimental

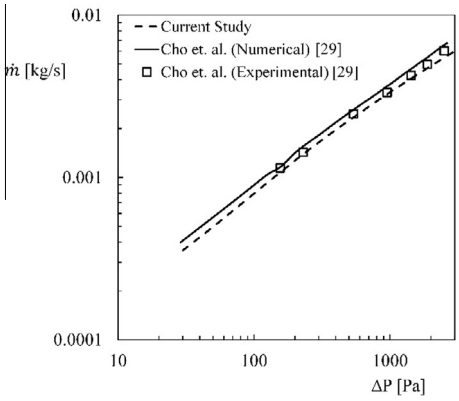

Fig. 2. Validation of the current numerical method with the results of Cho et al. [29].

setup and its photograph. The setup consists of three main parts; circulator cooling bath, test section and data acquisition system. The coolant fluid is distilled water, and there is no phase change. Circulatory consists of a heated/cooled bath (Labo C200-H13) with the temperature range of −20/+100 °C, the temperature stabilization of it is ±0.03 °C, and the volumetric flow rate of it can be as high as 13 l/min. A needle valve was mounted in the coolant line, which is also shown in Fig. 3, in order to control the flow rate precisely. In addition, a turbine flowmeter (ultra-low flow sensor ULF) with the range of 0.025–1.67 l/min and the accuracy of 1% was inserted in the coolant line. The maximum flow rate in the coolant section is 0.42 l/min, which is in the range of the inserted turbine flowmeter. Pulse output of the flowmeter was stored with a data logger (Hioki LR8431-20 hi-logger), which was also used for storing the temperature data of the ambient and coolant at the inlet and outlet of the vascular plate, via K-type thermocouples. These

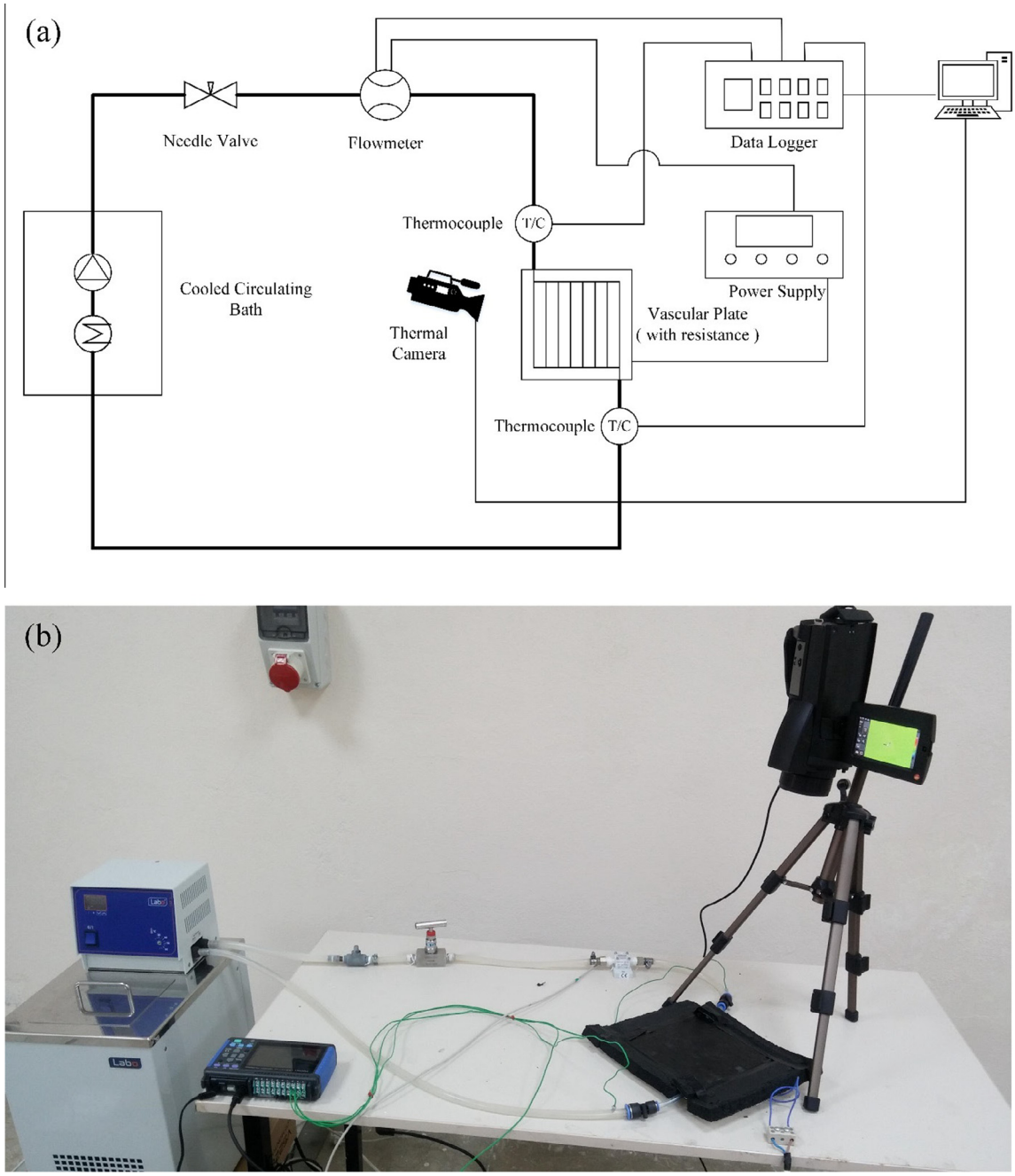

Fig. 3. (a) The schematic and (b) the photograph of the experimental setup.

thermocouples are consists of NiCr (+) and NiAl (−) conducting wires with 2 × 0.50 mm diameters, and their accuracy is 0.1 °C. The accuracy of the thermocouples was confirmed by measuring the temperature of a known temperature reservoir with them. In addition, the positions of the thermocouples in the inlet and outlet channels are changed in the vertical direction in order to confirm that the temperature distribution is uniform in the channels (the temperature differences at the different vertical positions are maximum 0.1 °C, hence; the measured temperature is considered as the mean temperature at the inlet and outlet ports).

The vascular plates were manufactured from 5083 Aluminum. The vascular channels were manufactured on top of each plate with precision CNC (computer numerical controlled) milling machine as semi-circular channels on top the plates. Afterwards, two Aluminum plates were adhered together with metal epoxy to form the vascularized structure, which can be seen in Fig. 4b, along with the open form of the vascular plate, Fig. 4a. Vascular plates were coated with black film, as shown in Fig. 4c, due to the low emissivity of aluminum, which can cause misreading from the thermal camera. In addition, the emissivity value of the coated vascular plates in the thermal camera (Testo 855-2) was calibrated by comparing the temperature values on top of the plate with thermocouple measurements. Furthermore, the vascular plate is placed on top of a silicone flexible resistance which is insulated at the bottom surface. The silicone flexible resistance with two different constant heat loads (50 W and 150 W) were used in the experiments.

While the experiments were being conducted for a cooling plate, the maximum temperature on the surface of the plate, the volumetric flow rate, ambient temperature and inlet/outlet water temperatures were stored in the data logger. In addition, these values were also monitored for the time dependency (i.e., when system reaches to steady state conditions). The numerical and experimental results are compared for the steady state case.

Detailed uncertainty analysis for the measurement instruments and various variables were made according to Figliola and Beasley [39]. The propagation of uncertainty method is used,

$$u_R = \left[\left(\frac{\partial R}{\partial x_1} u_1 \right)^2 + \left(\frac{\partial R}{\partial x_2} u_2 \right)^2 + \ldots\ldots + \left(\frac{\partial R}{\partial x_n} u_n \right)^2 \right] \quad (6)$$

where u_R is the uncertainty of $R = R(x_1, x_2, \ldots, x_n)$, a functional relationship of independent variables x_n and u_n are the uncertainties of independent variables x_n. Total uncertainties calculated for the flow rate, thermal camera and Reynolds number are ±3.42%, ±0.62% and ±3.42%, respectively.

4. Parallel channels design

Consider the parallel cooling channel design of Fig. 1 with circular channels and 120 × 120 mm AISI 304 stainless steel plates, which is exposed to a heat load of 5000 W/m^2. In order to uncover the effects of volume fraction (φ) on the cooling performance of the parallel channels, φ was varied such as 3.5%, 6.5%, 5% and 8% in the numerical simulations. The different volume fractions were obtained by increasing or decreasing the diameter of the channels while the number of channels and the design is fixed. The diameter of the main distributing and collecting channels were fixed to 0.003338 and 0.004 for the plates of 120 × 120 mm and 170 × 170 mm, respectively, as shown in Table 2. Fig. 5a shows that how the peak temperature varies when pressure drop varies between 30 Pa and 250 Pa for the volume fractions of φ = 0.035, 0.05, 0.065 and 0.08, when the number of channel is ten. The peak temperature decreases as the volume fraction increases, Fig. 5a. The reason for this decrease is that the resistances to the fluid flow decreases as channel diameters increase, and therefore the fluid gains greater access to the entire domain (i.e., convective and conductive resistances decrease). In addition, the surface area of the

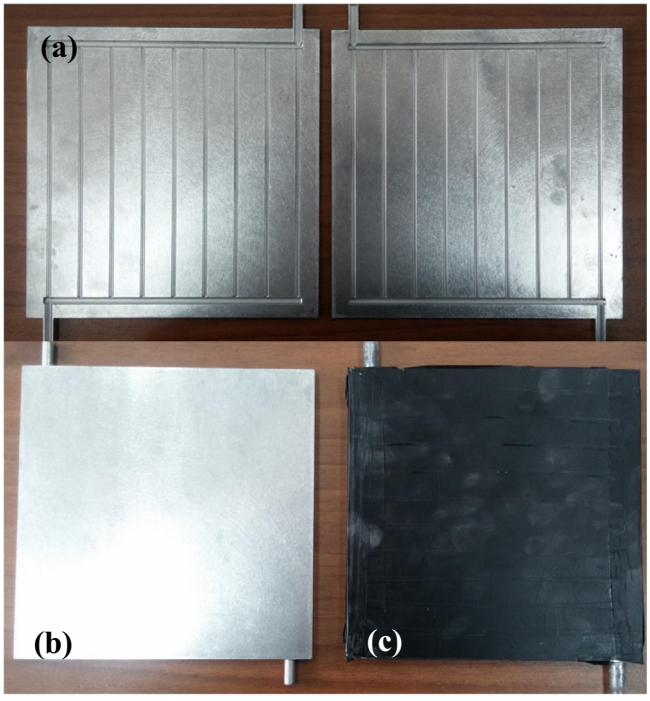

Fig. 4. (a) The open, (b) the closed, (c) and the coated form of the vascularized plate.

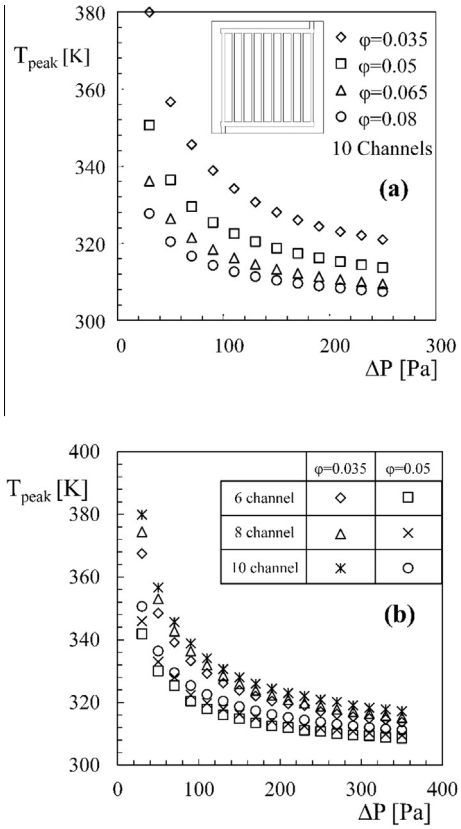

Fig. 5. Numerical results of the peak temperature variation relative to pressure drop (a) for parallel channels design with φ = 0.035, 0.05, 0.065 and 0.08, (b) for parallel channels design with 6, 8 and 10 number of channels when φ = 0.035 and 0.05.

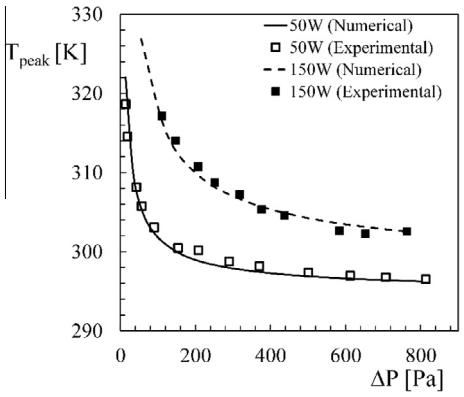

Fig. 6. Peak temperatures relative to pressure drop for experimental and numerical studies of parallel channels design with heat loads of 50 W and 150 W.

cooling channels also increase, which increases the overall heat transfer rate. Fig. 5 shows that as the pressure drop increases the peak temperature becomes independent of the changes in the pressure drop. In addition, our previous study [27] also shows that for a similar design this limit value is around 300 Pa.

Next, consider the circular parallel channels design with six and eight daughter channels in addition to ten, Fig. 5b. In order to have cooling channel diameters less than thickness of the plate, $\varphi = 0.035$ and $\varphi = 0.05$ are documented. Fig. 5b shows that the flow resistances to the heat flow with six daughter channels are smaller than the design with eight and ten daughter channels as ΔP varies from 30 Pa to 350 Pa. This is expected due to the diameter of the cooling channels increase as the number of channels decreases, i.e., T_{peak} decreases as the number of channels decrease from 10 to 8 and 6. This means that for a specified volume fraction, the effects of the conductive resistances due to the spacing in between the channels are negligibly small in comparison with the effect of the convective resistances. Fig. 5b also shows that the peak temperature decreases as the volume fraction increases. In addition, the comparison of the Fig. 5a and b shows that the effect of the volume fraction and the number of channels on the peak temperature is more apparent with low pressure drops such as in between 30 Pa and 100 Pa. Increasing the volume fraction and the number of channels in this pressure drop region can yield a change in the peak temperature. However, the volume fraction should be carefully increased in order to eliminate penetration of the plate walls by cooling channels.

Next, consider the parallel cooling channel design with 170×170 mm Aluminum vascularized plates with volume fraction of $\varphi = 0.05$. Fig. 6 documents the relation between the peak temperature and the pressure drop for experimental and numerical studies with heating loads of 50 W and 150 W. The experimental procedure was discussed in Section 3. Fig. 6 shows that the results of the numerical and experimental studies agree, the maximum relative errors are 0.88% and 0.39% for 50 W and 150 W, respectively. In addition, these differences are in between the calculated values in uncertainty analysis. The volumetric flow rate is limited as 7×10^{-6} m^3/s, i.e., the flow is laminar. In addition,

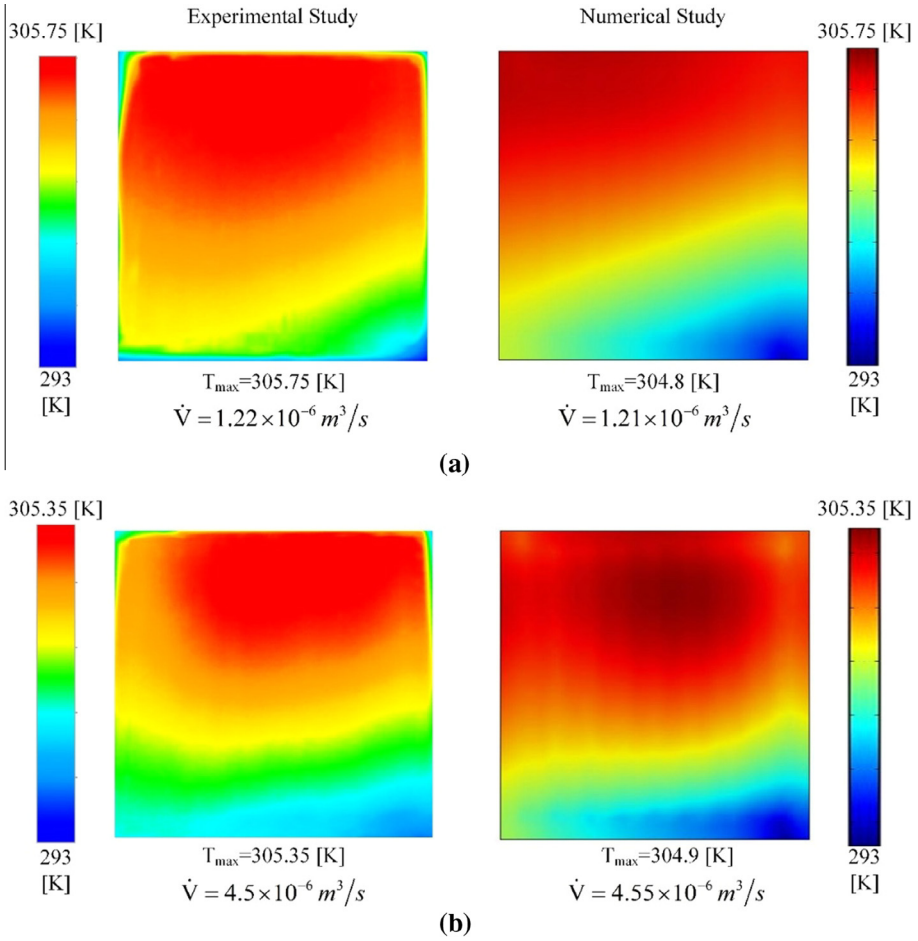

Fig. 7. Temperature distributions of parallel channels design for experimental and numerical studies with (a) 50 W (b) 150 W of heat loads.

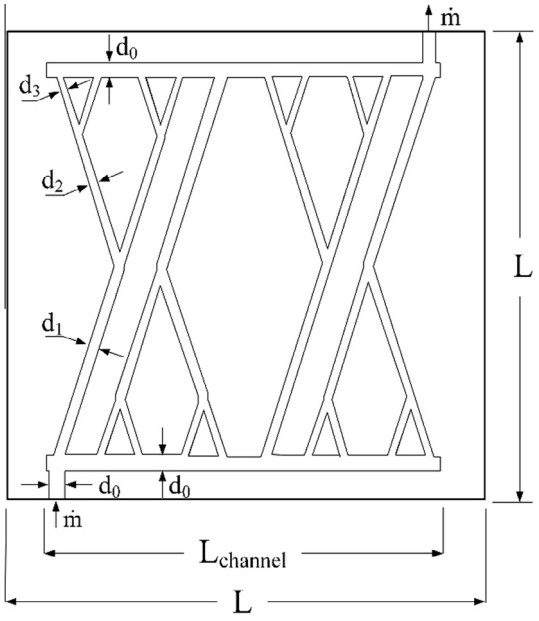

Fig. 8. Tree-shaped design configuration.

increasing the pressure drop after 350 Pa does not decrease the peak temperature more than several percent as discussed in the numerical results of Fig. 5.

Fig. 7 illustrates the temperature distributions of the numerical and experimental studies, for two heating loads: 50 W and 150 W. Similar to Fig. 6, Fig. 7 shows the agreement between the numerical and experimental studies. In addition, Fig. 7a shows that the peak temperature on the vascular plate surface are located close to the outlet channel for low volumetric flow rates. Because the temperature of the coolant fluid is already increased as it reaches to the collecting channel at the outlet port, therefore it cannot cool the vascular plate down as desired. Fig. 7b shows that the coolant fluid cools the vascular plate more homogeneously as the flow rate increases, in comparison to the Fig. 7a. Note that the peak temperature values are similar in Fig. 7a and b because the heating loads are 50 W and 150 W, respectively.

5. Tree-shaped design

Next, consider a tree-shaped design with three levels of embedded vascular cooling channels as shown in Fig. 8. The coolant fluid enters from the distributing channel of diameter d_0, and then it is distributed to the vascular channels of diameter d_1, d_2 and d_3, respectively or vice versa. At the junctions, the channels of diameter d_1 bifurcate into two daughter channels of diameter d_2, then the channels of diameter d_2 bifurcate into two daughter channels of diameter d_3. The diameter ratios at the junctions are determined according to the Hess–Murray Rule [36] as shown in Eq. (7). The root and branch channels are connected to the main collecting and distributing channels with equidistant ports, i.e. the location of the connection ports is the same with the parallel channel configuration. The length of the channels is constrained with the port locations and the number of the ports. The channel lengths were chosen in order to conform these constraints and not to intersect with each other.

$$d_i/d_{i+1} = 2^{1/3} \tag{7}$$

Now consider that the tree-shaped design in Fig. 8 with L = 120 mm, and it is exposed to a heat load of 5000 W/m^2. The resistance to the fluid flow decreases with the tree-shaped channel configuration in comparison to parallel channels configuration, i.e., mass flow rate increases in between 9.25% and 18.9% in tree-shaped configurations in comparison to the parallel channels configurations while pressure drop is fixed. This result is in accord with the current literature [23,24,35].

Fig. 9 shows how the peak temperature varies relative to the pressure drop for two competing designs: parallel channels and tree-shaped. In addition to the ten ports connected to the collecting and distributing channels, Fig. 9 also uncovers how the thermal performance is affected by the pressure drop when six ports connected to them. In parallel channels design, there are six parallel

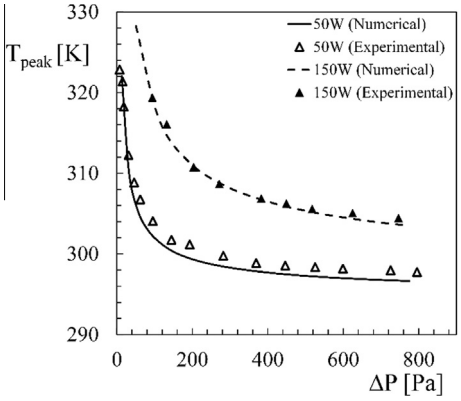

Fig. 10. Peak temperatures relative to the pressure drop for experimental and numerical studies of tree-shaped design for heat loads of 50 W and 150 W.

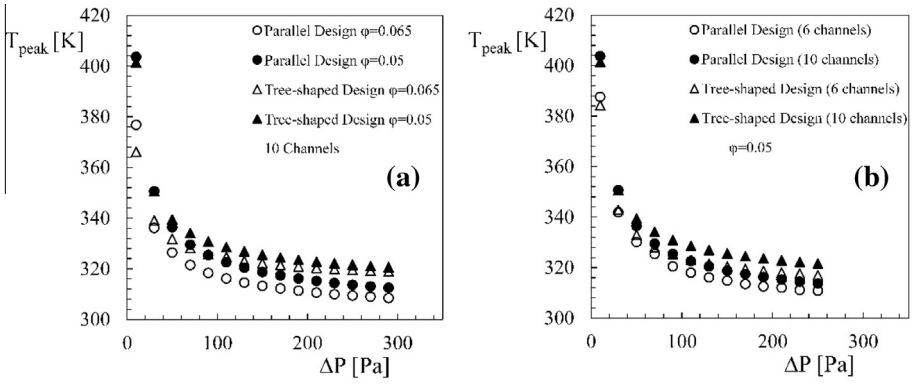

Fig. 9. Numerical results of the peak temperature relative to the pressure drop for tree-shaped and parallel channels designs for (a) 10 daughter channels with φ = 0.065 and φ = 0.05 (b) 6 and 10 daughter channels with φ = 0.05.

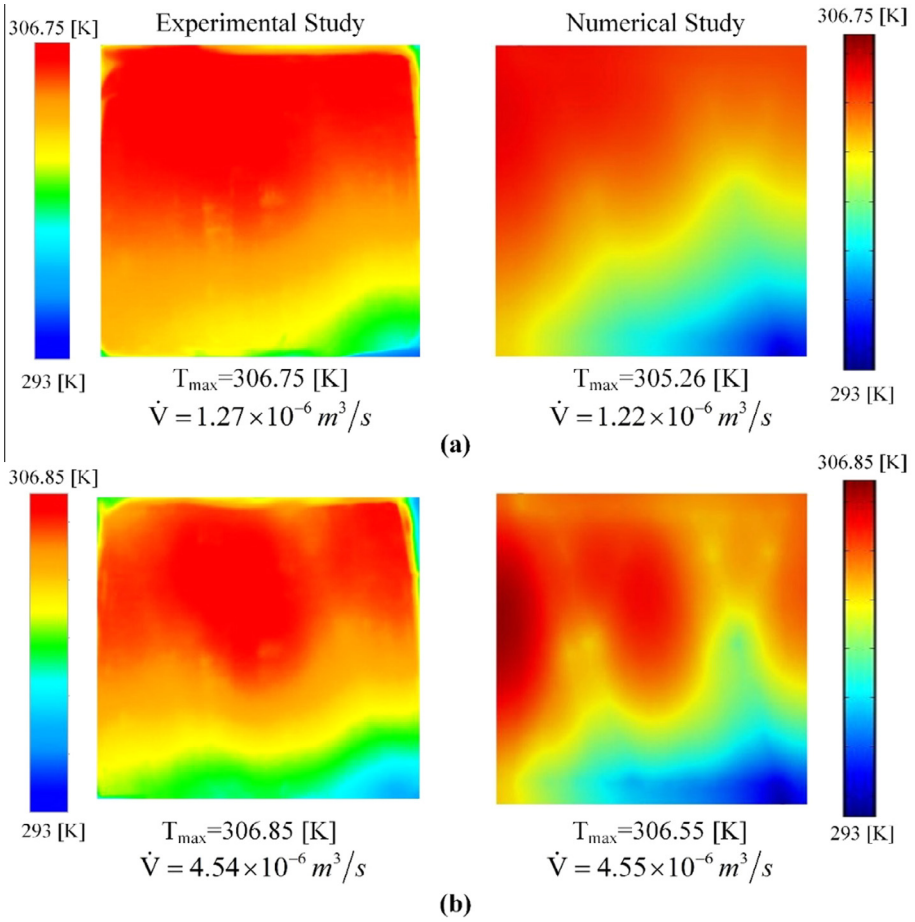

Fig. 11. Temperature distributions of tree-shaped design for experimental and numerical studies with (a) 50 W (b) 150 W of heating loads.

channels which are connected to the distributing and collecting channels of diameter d_0. The tree-shaped designs of one bifurcation level are also connected to the distributing and collecting channels of diameter d_0, i.e., the channels of diameter d_1 bifurcates into channels of diameter d_2 at the junctions (the channels of diameter d_3 is absent in Fig. 8).

First, the effect of pressure drop on the peak temperature for parallel channels and tree-shaped designs with $\varphi = 0.05$ and $\varphi = 0.065$ is shown in Fig. 9a. The peak temperature is smaller with tree-shaped design for a pressure drop of 10 Pa, and the peak temperature is smaller with parallel channels design when pressure drop varies in between 30 Pa and 290 Pa. Next, Fig. 9b shows how the peak temperature is affected when the number of vascular channel inlet ports are decreased from ten to six when $\varphi = 0.05$. The volume fraction was decreased from $\varphi = 0.065$ to $\varphi = 0.05$ in order to have smaller channel diameters than the thickness of the plate. However, the effect of design governs the peak temperature, and the effects of number of channels (from 6 to 10) and volume fraction (from 0.05 to 0.065) diminish as shown in Fig. 9.

Fig. 10 shows how the peak temperature varies relative to the pressure drop for tree-shaped design with 170 × 170 mm Aluminum vascular plates for heating loads of 50 W and 150 W. The results of experimental and numerical studies are in agreement, i.e., 0.49% and 0.23% maximum relative errors on peak temperature for 50 W and 150 W, respectively. The peak temperature shows an exponential decay relative to the increase in the pressure drop. First, a sudden decrease in the peak temperature is observed up to 200 Pa and 400 Pa pressure drop values for 50 W and 150 W heat loads, respectively. Then, the peak temperature becomes

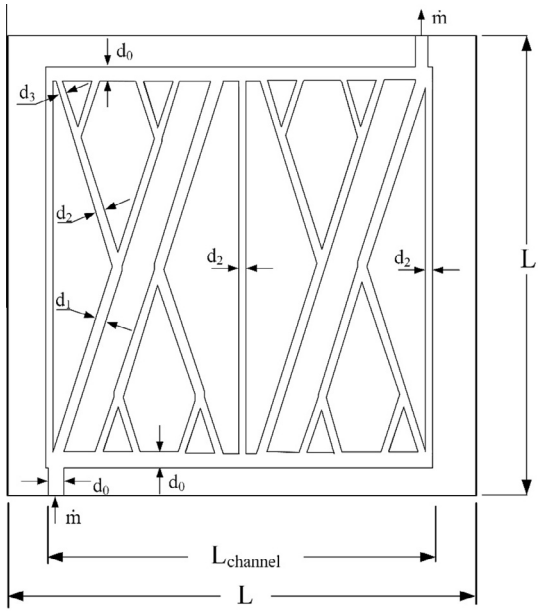

Fig. 12. Hybrid design.

independent of the increase in the pressure drop. The reason of this behavior is related with the cooling capability of the coolant. As the pressure drop (flow rate) increases the capacitance of the coolant

also increase. However, there is a limit value for the pressure drop as shown in Fig. 10 because the time for coolant to pass along the vascular channels also decrease as the flow rate increases.

In addition, Fig. 11 shows the temperature distributions of the tree-shaped design, for experimental and numerical studies for two heating loads (50 W and 150 W). For $\dot{V} = 1.27 \times 10^{-6}$ m^3/s, the temperature distribution is similar with the parallel channels design, the peak temperatures are located around collecting channels. However, for $\dot{V} = 4.54 \times 10^{-6}$ m^3/s, the peak temperatures are located in between the tree-shaped channels where there is no embedded cooling channels. This result shows that the conductive resistances become essential in the tree-shaped design as the pressure drop increases.

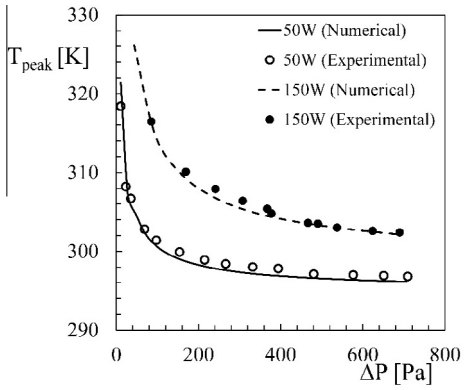

Fig. 13. Peak temperatures relative to pressure drop for experimental and numerical studies of hybrid design for heat loads of 50 W and 150 W.

6. Hybrid design

In our previous study [27], we suggested a hybrid design of parallel channels and tree-shaped designs because both designs are superior to each other by means of heat and fluid flow performances, respectively. The hybrid design was constructed by adding parallel channels to the uncooled regions of the tree-shaped design as shown in Fig. 12. Our previous study showed numerically that the hybrid design performs similar to the parallel channels design in terms of thermal performance and similar to the tree-shaped design in terms of resistances to the fluid flow, i.e., combining best features of both designs [27].

Consider the hybrid design of Fig. 12 made of Aluminum with the plate size of 170 × 170 mm. Fig. 13 shows the thermal performance of the hybrid design for both experimental and numerical studies for two different heat loads (50 W and 150 W). The comparison shows that there is a good agreement, i.e., 0.94% and 0.22% maximum relative errors between experimental and numerical studies, for 50 W and 150 W of heat loads, respectively. The maximum relative errors are in between the calculated values in uncertainty analysis. In addition, the peak temperature does not decrease more than several percent when the pressure drop is higher than 200 Pa.

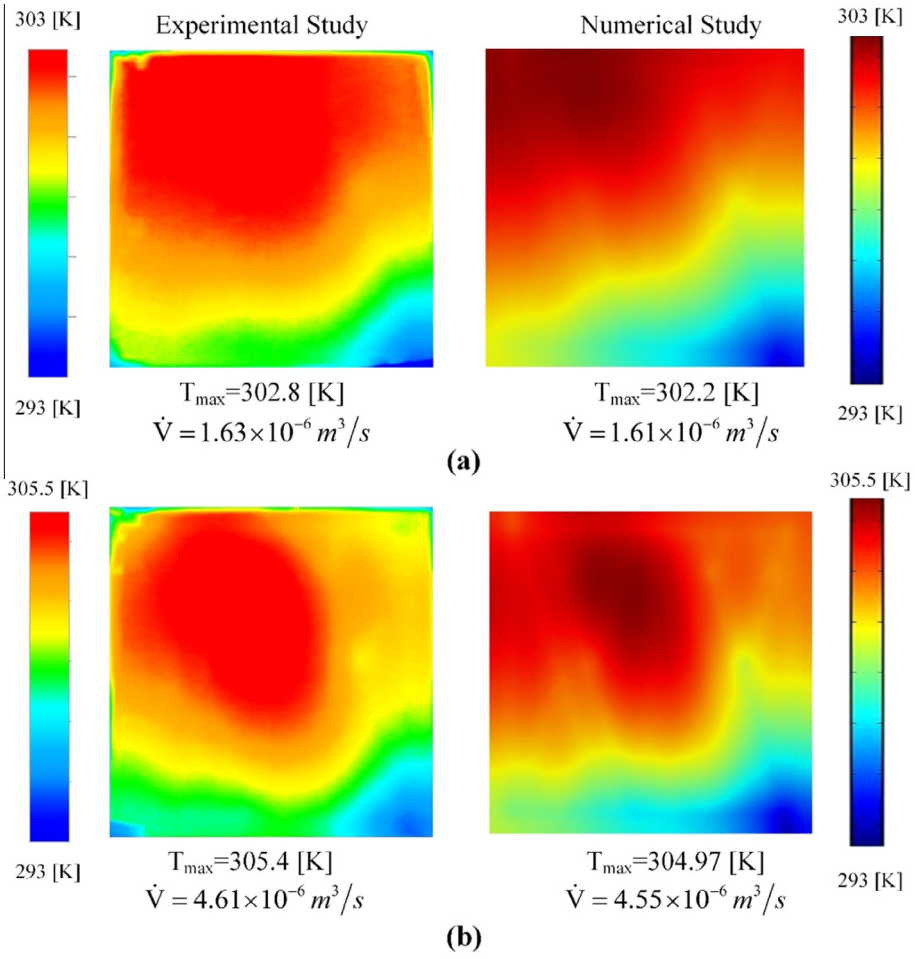

Fig. 14. Temperature distributions of hybrid design for experimental and numerical studies with (a) 50 W (b) 150 W of heating loads.

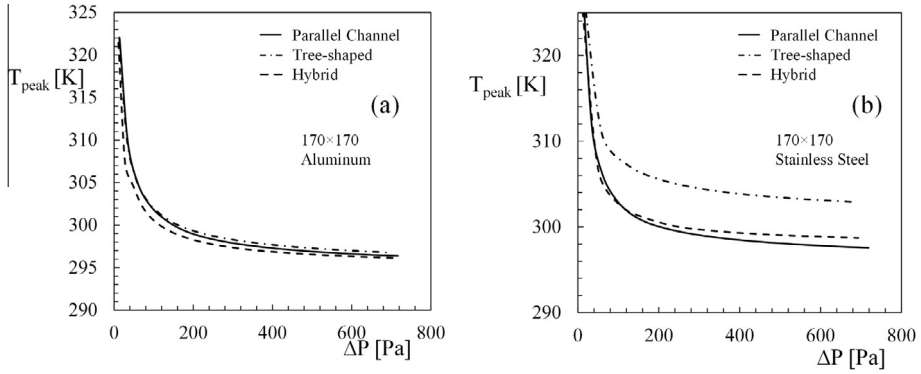

Fig. 15. Numerical results of the peak temperatures relative to the pressure drop for the three competing designs with (a) Aluminum and (b) Stainless Steel plates.

Next, Fig. 14 shows the temperature distributions of numerical and experimental studies for 50 W and 150 W heating loads. Similar to the parallel channels and tree-shaped designs, the hot spots are located near the outlet channel in hybrid design as shown in Fig. 14a. The comparison of Figs. 11b and 14b shows that the peak temperature decreases with the additional parallel channels introduced in the hybrid design. However, the hot spot is located in between the tree-shaped branches and close to the main collecting channel in hybrid design as shown in Fig. 14b. Therefore, increasing the diameter of the parallel channel placed in between the tree-shaped branches in hybrid design may further decrease the peak temperature. In addition, the results of experimental and numerical studies are in agreement as can be seen from Fig. 14.

Fig. 15 shows the comparison of the thermal performances of the three competing designs; parallel channels, tree-shaped and hybrid designs, with (a) Aluminum 170 × 170 mm vascular plates and (b) Stainless Steel 170 × 170 mm vascular plates, when the heat load is 50 W. Fig. 15a shows that the peak temperature is minimum with the hybrid design, which is more significant when the pressure drop is changing from 40 Pa to 400 Pa (peak temperature is 1% lower with hybrid design than with the parallel channels design), after that point the design effect diminishes and all designs performs almost the same (the peak temperature changes less than 0.01%) because the effect of convective resistances becomes negligibly small in comparison with the conductive resistances.

In order to uncover the effect of material on the thermal performance, the studies were repeated for AISI-304 stainless steel. Fig. 15b shows how the peak temperature varies relative to the pressure drop for stainless steel vascular plates. Unlike in Fig. 15a, 15b shows that the effect of design on the peak temperature is visible, i.e., tree-shaped design has maximum 1.8% and 1.5% greater peak temperatures in comparison to parallel channels and hybrid designs, respectively. The reason for this change is due to the increase in the conductive thermal resistances (thermal conductivity of stainless steel is almost twelve times less than the thermal conductivity of Aluminum). Therefore, the effect of uncooled regions creates a non-uniform temperature distribution in the tree-shaped design in comparison to the other designs. The thermal performance of the parallel channels design is slightly better than the performance of the hybrid design (peak temperature is 0.5% less) as pressure drop becomes more than 100 Pa. When the pressure drop is less than 100 Pa, the peak temperature is minimum with the hybrid design as shown in Fig. 15a and b. For the same pressure drop value, flow rate is greater in the hybrid design than in the parallel channels design. Therefore, the peak temperature is minimum with the hybrid design when the pressure drop is less than 100 Pa, even though the conductive resistances are greater in the hybrid design than in the parallel channels design. Fig. 15a and b show that changing only the material changes the best performing vascular channel network which is not evident in non-dimensional simulation results. Tree-shaped and hybrid designs show better thermal performance than parallel channel designs as the thermal conductivity of the material increases. The reason of this behavior is due to the greater spacing in between the cooling channels in tree-shaped and hybrid designs than in parallel channels, i.e. the effect of conductive resistances in between channels diminishes as the thermal conductivity increases.

7. Conclusion

Here, we showed that a plate on which heating load is applied can be kept under a desired temperature level with vascular channels. The effect of the volume fraction and the number of channels on cooling performance for parallel channels and tree-shaped designs are documented. Tree-shaped configurations provide smaller flow resistances than the parallel channels configurations for the same volume fraction. Therefore, the peak temperature is minimum with tree-shaped configurations when the pressure drop is small (i.e., 10 Pa as shown in Fig. 9). However, the conductive thermal resistances are greater in tree-shaped configurations than in parallel channels configurations. Therefore, the parallel channel configurations provide better cooling performance as the pressure drop increases. In addition, the thermo-fluidic performance of the vascularized plates with parallel channels and tree-shaped designs were also studied experimentally. Then, the results were compared with the numerical results, and the maximum relative error for peak temperatures on the top surface are 0.88% and 0.49% for parallel channels and tree-shaped designs, respectively. Furthermore, the temperature distributions of numerical and experimental studies were compared, which shows that the numerical results are in good agreement with the experimental results.

Then, the thermo-fluidic performance of the hybrid design was surveyed both experimentally and numerically. The maximum relative error is 0.94%. The thermal performance of all competing designs were compared. We have found that the hybrid design in Aluminum plates provides the smallest peak temperature (or close to the smallest peak temperature) and the highest volume flow rate for the entire pressure drop region. Furthermore, the same comparison made for stainless steel vascular plates in order to uncover the effect of material on cooling performance.

Overall, this paper shows how a plate can be vascularized for enhancing the thermal conductance. The results were validated with experiments, and the effect of material on the thermal performance and optimum vascular channel design selection were

uncovered. Here we showed that each design is superior to the others for a specific set of objective and conditions.

Acknowledgement

This research was funded by the scientific and technological research council of Turkey (TUBITAK) under grant number 114M592.

References

[1] E. Cetkin, Inverted fins for cooling of a non-uniformly heated domain, J. Therm. Eng. 1 (1) (2015) 1–9.
[2] E. Cetkin, A. Oliani, The natural emergence of asymmetric tree-shaped pathways for cooling of a non-uniformly heated domain, J. Appl. Phys. 118 (2015) 024902.
[3] S.M. Senn, D. Poulikakos, Laminar mixing, heat transfer and pressure drop in tree-like microchannel nets and their application for thermal management in polymer electrolyte fuel cells, J. Power Sources 130 (2004) 178–191.
[4] S.M. Senn, D. Poulikakos, Tree network channels as fluid distributors constructing double-staircase polymer electrolyte fuel cells, J. Appl. Phys. 96 (1) (2004) 842–852.
[5] L. Luo, Y. Fan, D. Tondeur, Heat exchanger: from micro- to multi-scale design optimization, Int. J. Energy Res. 31 (2007) 1266–1274.
[6] X. Wei, Y. Joshi, M.K. Patterson, Experimental and numerical study of a stacked microchannel heat sink for liquid cooling of microelectronic devices, J. Heat Transfer 129 (2007) 1432–1444.
[7] M.G. Khan, A. Fartaj, Heat exchanger: a review on microchannel heat exchangers and potential applications, Int. J. Energy Res. 35 (2011) 553–582.
[8] A. Sakanova, C. Keian, J. Zhao, Performance improvements of microchannel heat sink using wavy channel and nanofluids, Int. J. Heat Mass Transf. 89 (2015) 59–74.
[9] A.A. Minea, Numerical studies on heat transfer enhancement and synergy analysis on few metal oxide water based nanofluids, Int. J. Heat Mass Transfer 89 (2015) 1207–1215.
[10] M. Shafahi, V. Bianco, K. Vafai, O. Manca, Thermal performance of flat-shaped heat pipes using nanofluids, Int. J. Heat Mass Transfer 53 (2010) 1438–1445.
[11] Y. Li, H.Q. Xie, W. Yu, J. Li, Liquid cooling of tractive lithium ion batteries pack with nanofluids coolant, J. Nanosci. Nanotechnol. 15 (4) (2015) 3206–3211.
[12] W.G. Alshaer, S.A. Nada, M.A. Rady, E.P. Del Barrio, A. Sommier, Thermal management of electronic devices using carbon foam and PCM/nano-composite, Int. J. Therm. Sci. 89 (2015) 79–86.
[13] T. Li, J. Lee, R. Wang, Y.T. Kang, Heat transfer characteristics of phase change nanocomposite materials for thermal energy storage application, Int. J. Heat Mass Transfer 75 (2014) 1–11.
[14] T. Ma, H.X. Yang, Y.P. Zhang, L. Lu, X. Wang, Using phase change materials in photovoltaic systems for thermal regulation and electrical efficiency improvement: a review and outlook, Renewable Sustainable Energy Rev. 43 (2015) 1273–1284.
[15] E. Cetkin, S. Lorente, A. Bejan, Vascularization for cooling a plate heated by a randomly moving source, J. Appl. Phys. 112 (8) (2012) 084906.
[16] S. Kim, S. Lorente, A. Bejan, Vascularized materials: tree-shaped flow architectures matched canopy to canopy, J. Appl. Phys. 100 (2006) 063525.
[17] J. Lee, S. Kim, S. Lorente, A. Bejan, Vascularization with trees matched canopy to canopy: diagonal channels with multiple sizes, Int. J. Heat Mass Transfer 51 (2008) 2029–2040.
[18] S. Kim, S. Lorente, A. Bejan, W. Miller, J. Morse, The emergence of vascular design in three dimensions, J. Appl. Phys. 103 (2008) 123511.
[19] K.M. Wang, S. Lorente, A. Bejan, Vascular materials cooled with grids and radial channels, Int. J. Heat Mass Transfer 52 (5–6) (2009) 1230–1239.
[20] S.R. White, N.R. Sottos, P.H. Geubelle, J.S. Moore, M.R. Kessler, S.R. Sriram, E.N. Brown, S. Viswanathan, Autonomic healing of polymer composites, Nature 409 (2001) 794–797.
[21] A. Bejan, S. Lorente, K.M. Wang, Networks of channels for self-healing composite materials, J. Appl. Phys. 100 (3) (2006) 033528.
[22] S. Kim, S. Lorente, Bejan, Dendritic vascularization for countering intense heating from the side, Int. J. Heat Mass Transfer 51 (2008) 5877–5886.
[23] J. Lee, S. Lorente, A. Bejan, Transient cooling response of smart vascular materials for self-cooling, J. Appl. Phys. 105 (2009) 064904.
[24] L.A.O. Rocha, S. Lorente, A. Bejan, Tree-shaped vascular wall designs for localized intense cooling, Int. J. Heat Mass Transfer 52 (19–20) (2009) 4535–4544.
[25] J. Lee, S. Lorente, A. Bejan, Vascular design for thermal management of heated surface, Aeronaut. J. 113 (1144) (2009) 397–407.
[26] E. Cetkin, S. Lorente, A. Bejan, Hybrid grid and tree structures for cooling and mechanical strength, J. Appl. Phys. 110 (6) (2011) 064910.
[27] O. Yenigun, E. Cetkin, Constructal tree-shaped designs for self-cooling, Int. J. Heat Technol. 34 (2016) 173–178.
[28] K.-H. Cho, J. Lee, H.S. Ahn, A. Bejan, M.H. Kim, Fluid flow and heat transfer in vascularized cooling plates, Int. J. Heat Mass Transfer 53 (19–20) (2010) 3607–3614.
[29] K.-H. Cho, W.-P. Chang, M.-H. Kim, A numerical and experimental study to evaluate performance of vascularized cooling plates, Int. J. Heat Fluid Flow 32 (2011) 1186–1198.
[30] K.M. Wang, S. Lorente, A. Bejan, Vascular structures for volumetric cooling and mechanical strength, J. Appl. Phys. 107 (2010) 044901.
[31] E. Cetkin, S. Lorente, A. Bejan, Vascularization for cooling and mechanical strength, Int. J. Heat Mass Transfer 54 (13–14) (2011) 2774–2781.
[32] L.A.O. Rocha, S. Lorente, A. Bejan, Vascular design for reducing hot spots and stresses, J. Appl. Phys. 115 (17) (2014) 174904.
[33] E. Cetkin, S. Lorente, A. Bejan, Vascularization for cooling and reduced thermal stresses, Int. J. Heat Mass Transfer 80 (2015) 858–864.
[34] E. Cetkin, Constructal vascular structures with high-conductivity inserts for self-cooling, J. Heat Transfer 137 (2015). 111901-1.
[35] A. Bejan, S. Lorente, Design with Constructal Theory, John Wiley & Sons, 2008.
[36] A. Bejan, J.P. Zane, Design in Nature, Anchor Books, 2013.
[37] A. Bejan, Physics of Life, St. Martin's Press, 2016.
[38] COMSOL Multiphysics 5.0, COMSOL Inc., 2014.
[39] R.S. Figliola, D.E. Beasley, Theory and Design for Mechanical Measurements, John Wiley & Sons, 2011.